energies

MDPI

Article

Effect of the Particle Size on the Near-Wall Turbulence Characteristics of the Polymer Fluid Flow and the Critical Velocity Required for Particle Removal from the Sand Bed Deposited in Horizontal Wells

Mehmet Meric Hirpa †, Sumanth Kumar Arnipally and Ergun Kuru *

School of Mining & Petroleum Engineering, University of Alberta, Edmonton, AB T6G 1H9, Canada; hirpa@ualberta.ca (M.M.H.); arnipall@ualberta.ca (S.K.A.)

* Correspondence: ekuru@ualberta.ca; Tel.: +1-780-492-2025

† Now with Fourquest Energy.

Received: 1 May 2020; Accepted: 16 June 2020; Published: 18 June 2020

Abstract: Water-based polymer drilling fluids are commonly used for drilling long horizontal wells where eliminating the drilling fluid-related formation damage and minimizing the environmental impact of the drilling fluids are the main concerns. An experimental study was conducted to investigate the turbulent flow of a polymer fluid over a stationary sand bed deposited in a horizontal pipeline. The main objectives of the study were to determine the effects of sand particle size on the critical velocity required for the onset of the bed erosion and the near-wall turbulence characteristics of the polymer fluid flow over the sand bed. Industrial sand particles having three different size ranges (20/40, 30/50, 40/70) were used for the experiments. The particle image velocimetry (PIV) technique was used to determine instantaneous local velocity distributions and near-wall turbulence characteristics (such as Reynolds stress, axial and turbulence intensity profiles) of the polymer fluid flow over the stationary sand bed under turbulent flow conditions. The critical velocity for the onset of the particle removal from a stationary sand bed using a polymer fluid flow was affected by the sand particle size. The critical velocity required for the particle removal from the bed deposits did not change monotonously with the changing particle size. When polymer fluids were used for hole cleaning, the particle size effect on the critical velocity varied (i.e., critical velocity increased or decreased) depending on the relative comparison of the sand particle size with respect to the thickness of the viscous sublayer under turbulent flow condition.

Keywords: drilling fluids; hole cleaning; horizontal wells; turbulent flow; PIV; particle size

1. Introduction

The deposition of drilled cuttings on the low side of the well is inevitable when drilling long horizontal or extended reach wells. If the cuttings are not sufficiently cleaned, operational problems such as slow drilling rate, excessive torque and drag, bridging, pack-off, hole fill, and a pipe stuck would occur [1–3]. Drilling needs to be interrupted occasionally to clean the well from cuttings, however, this costs time and money.

Hole cleaning and the bed erosion process in annular geometry have been extensively studied in the past. Brown et al. [4] studied the hole-cleaning performance of water and some polymer-based fluids through a set of experiments conducted using a specially designed flow loop. Martins et al. [5] conducted extensive experiments to study stratified solid–liquid annular flow. In an effort to determine the critical shear stress required for cuttings movement, they have developed correlations for an interfacial friction factor and showed its dependency on the ratio of particle diameter to hydraulic

diameter, as well as fluid rheological properties. Martins et al. [6] also presented the results of extensive bed erosion tests conducted using different polymeric suspensions in annular flow, at several different flow rates, wellbore inclinations and drill pipe rotational speeds. Based on the experimental results, they have developed a method to quantify the volume of solids removed from the highly inclined and horizontal annulus with time. Adari et al. [7] carried out a number of experiments to determine the effects of the drilling fluid flow rate and rheological properties on the cuttings bed erosion. Cho et al. [8] proposed a mathematical model describing hole cleaning in the critical 30–60 degree inclination region. They have introduced the concept of minimum anti-sliding velocity of cuttings bed (MASV) based on the interrelationship between parameters, which involves fluid rheology, wellbore deviation angle, interfacial friction between the suspension layer and cuttings bed, and in situ fluid velocity in the suspension layer. Ozbayoglu et al. [9] conducted an extensive experimental study and by using some very innovative experimental techniques determined some of the very difficult-to-identify data (e.g., concentration of moving particles, their relative transport velocities, slip velocity between the phases, friction factor on the stationary bed, etc.) that are essential for models used for the accurate prediction of total pressure drop and total cuttings concentrations in the drilling of highly inclined and horizontal wells. Petersen [10] conducted a theoretical study to determine the most significant physical phenomena involved in establishing critical transport fluid velocity (CTFV, the minimum required fluid velocity to prevent the formation of stationary cuttings bed in inclined wells) and showed that physics-based equations can replace many of the empirical correlations suggested by previous studies. Several experimental studies have also been conducted to investigate the bed load transport and/or bed erosion of proppants in slick water hydraulic fracturing systems [11–14]. Interested readers should refer to the excellent reviews of the hole-cleaning literature provided by Li et al. [2,3] for further reading.

The efficiency of solids transport is controlled by multiple factors. The fluid rheological properties [7], flow rate [7], particle physical properties [15] and the flow geometry (i.e., eccentricity in the case of annulus) [16] are among the most important. Rheological properties of the transport fluid may improve or impede the solids transport efficiency [17]. Circulating the drilling fluid at any rate may not be adequate to disturb the deposited sand bed unless a critical flow rate and a shear stress threshold for bed erosion is exceeded [2,3]. However, the high-flow velocities required for keeping the solid particles in full suspension are not always applicable because of the potential borehole instability problems and limited pump pressure capacity. Bed load transport of particles, therefore, becomes one of the most common mechanisms for transporting drilled cuttings through the horizontal section of the wellbores as well as transporting solids in other oilfield applications such as the effective transport of proppants through hydraulically generated fractures [11–14,18]. McClure [11] describes the bed load transport as the particle movement over the bed deposits in rolling and saltation mode, under the effects of the viscous drag and turbulent lift forces. Better understanding of the hydrodynamics of the bed load transport process is needed for the design and development of hydraulic programs for the effective transport of drilled cuttings in horizontal wells and proppants in hydraulically generated fractures.

Bernoulli lift forces and the viscous drag forces are known to be the two main controlling forces that would keep solid particles in suspension under turbulent flow conditions [11]. Diplas et al. [19] investigated the importance of turbulent flow on bed erosion. Their results indicated that velocity fluctuations in turbulent flow are instrumental for the removal of the particles from stationary bed deposits. Bizhani and Kuru [20] investigated the effect of fluid velocity and turbulence on the hole cleaning by using the particle image velocimetry (PIV) technique. They have shown that the drag forces resulting from turbulent velocity fluctuations could be as high as the ones generated by the mean flow velocity. Results from studies like Diplas et al. [19], Bizhani and Kuru [20] and others all indicated that the turbulent flow is very critical for the efficient removal of solid particles from stationary bed deposits.

The chaotic nature of the turbulent flow coupled with the complex interaction of particles and the flow makes the theoretical treatment of the problem very difficult. Because there are many time and length scales, direct measurements of local fluid–particle interaction are needed in order to understand

the coupling of the phases. Micro-scale measurement techniques, such as particle image velocimetry (PIV) and particle tracking velocimetry (PTV) have been found useful to accomplish such complex tasks. Rabenjafimanantsoa et al. [21] studied the flow over the sand bed by using particle image velocimetry (PIV) and ultrasound velocity profile (UVP) techniques, which provided an improved understanding on the flow structure and its relationship to the sand bed. Bizhani and Kuru [20] studied the effect of fluid viscoelasticity on the bed erosion dynamics in horizontal annuli by using the PIV technique. They have reported that increasing fluid elasticity hindered the particle removal from sand bed deposits.

Particles size, density and surface characteristics are all expected to affect the dynamics of the bed erosion and the efficiency of the particle transport. The effect of particle density is generally well known. As the particle density increases, the gravity forces also increase, which makes the particle removal difficult. However, the effect of the particle size on the dynamics of the bed erosion has not been extensively studied. Ramadan et al. [18] investigated the bed load transport of the sand particles with different sizes in inclined wellbores. They conducted hole-cleaning experiments to determine the critical velocity for each sand size with water and polyanionic cellulose polymer (PAC) solutions. They also presented mechanistic models predicting the critical velocity when the transport fluid is water and a PAC solution.

Recently, Hirpa et al. [22] conducted a study where they investigated the effect of particle size on the sand bed erosion with water flow in a horizontal pipe. They reported that the critical velocity required for particle removal from the sand bed deposits significantly increased with the increasing particle size. This paper summarizes the results of a follow-up study, where we used a water-based polymer fluid for the particle removal from the sand bed deposited in a horizontal pipeline. The main objective was to study the effects of the sand particle size on the near-wall turbulence characteristics of the polymer fluid flow and the critical velocity required for the particle removal from the sand bed deposited in horizontal wells.

Previous studies [20,22] have shown that the critical velocity for particle removal from bed deposits monotonously increased with the increasing particle size, when water was used for hole cleaning. However, the particle size effect on the critical velocity was different when the polymer fluids were used. Contrary to bed erosion tests with water, previous studies [15] reported that small sized particles were more difficult to remove when polymer fluids were used for hole cleaning. In this study, by conducting bed erosion experiments under controlled conditions, we were able to explain the possible reasons (i.e., physical mechanisms responsible for this phenomena) for this contradicting behavior.

2. Materials and Methods

2.1. Sand Particles

The sand particles (SG = 2.65) of three different mesh sizes of 20/40, 30/50 and 40/70 were used in this study. Table 1 summarizes the range of particle sizes in microns.

Table 1. Size ranges of the sand particles used in the experiments.

Sand Particle Mesh Size	Sand Particle Size Range (Microns)
20/40	420–840
30/50	297–590
40/70	210–420

2.2. Fluids

A dilute (0.032% w/w) water-based solution of polyacrylamide (Alcomer RD 110) type of polymer was used in these experiments. The rheological properties of the polymer fluid were determined by using a high-resolution Bohlin C-VOR 150 rheometer. The rheogram (shear stress vs. shear rate plot) of

the polymer fluid is presented in Figure 1. The fluid shows pseudo plastic (power law) behavior with consistency index (K) and flow behavior index (n) values of 0.0055 (Pa·s^n) and 0.9093, respectively.

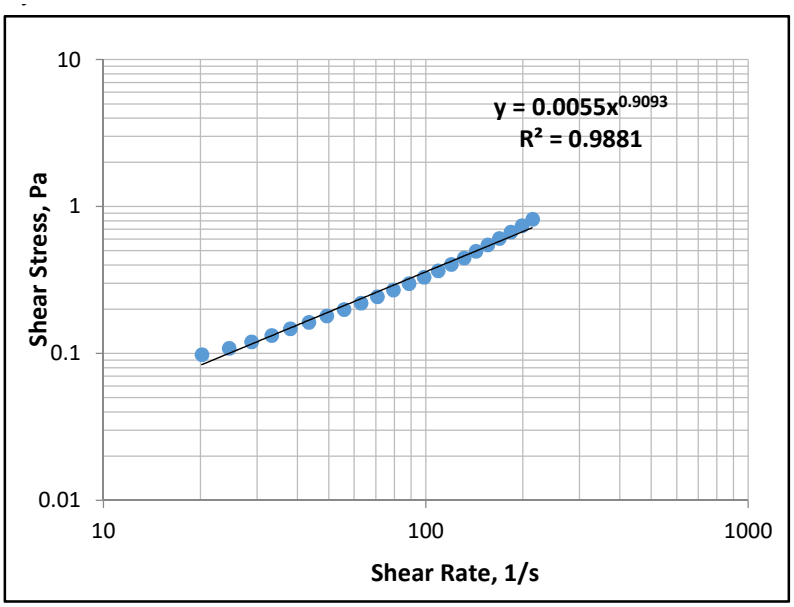

Figure 1. Rheogram of the polymer fluid used in the study.

2.3. Experimental Setup

A schematic view of the horizontal flow loop used in the bed erosion experiments is presented in Figure 2. The main elements of the flow loop are; a 500-L capacity mixing tank, a variable frequency drive (VFD) centrifugal pump, a differential pressure transducer, a magnetic flow meter, and several gate valves to control the fluid flow through the system and glass tubes.

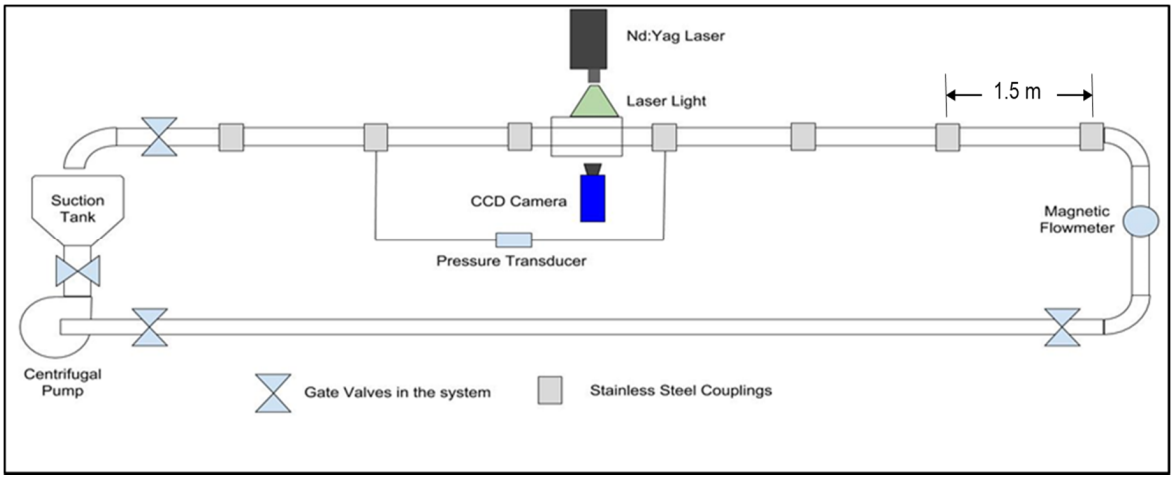

Figure 2. Schematic diagram of the experimental flow loop.

A VFD-controlled Gorman-Rupp self-priming centrifugal pump (model U4B60S-B/F), with a maximum operating pressure of 883 kPa (128 psi) and a maximum volumetric flow rate of 2500 lpm (660 gpm), was used for the hole-cleaning/bed erosion experiments. The 9 m long test section consisted of borosilicate glass pipes with 95 mm ID. The data acquisition system was operated by National Instrument's LabVIEW software (LabVIEW 2010). The flow rate was measured by OMEGA FMG607-R, a magnetic flow meter with an accuracy of ±0.5%, which was installed at the test section inlet. A differential pressure transducer, OMEGA DPG409, with an accuracy of ±0.08%, was used for the

measurement of the frictional pressure drop over the 3.08 m long pipe section. The first differential pressure tap line is located approximately ~48D downstream of the entrance to ensure that a fully developed flow is achieved (Length/Diameter ratio = 48).

Cengel and Cimbala [23] recommended the following equation to determine the minimum hydrodynamic entrance length required for establishing a fully developed turbulent flow:

$$L = 4.4D\,(Re)^{1/6} \quad (1)$$

We used the following generalized Reynolds number equation [24] given for power law type fluids:

$$Re = (\rho D^n \cdot u^{2-n})/(K \cdot ((3n + 1)/4n)^n \cdot 8^{n-1}) \quad (2)$$

where L (m) is the minimum entrance length required for achieving a fully developed turbulent flow, D (m) is the pipe inner diameter, ρ (kg/m^3) is the fluid density, u (m/s) is the fluid velocity, n is the flow behavior index, and K (Pa·s^n) is the consistency index. The highest L/D ratio required for achieving a fully developed turbulent flow under our polymer fluid flow experimental conditions was 23 (it was 29 for water flow). Therefore, it was safe to assume that the flow was fully developed before it reached to the point where the differential pressure loss measurement tap was installed.

Figure 3 shows the camera—laser alignment and the main test section used for recording the particle image velocimetry (PIV) data for all the bed erosion experiments. In this section, the borosilicate glass pipe was inside a rectangular glass box filled with glycerol. This way, measurement errors that may have arisen from the undesired refraction of the light passing through the circular pipe were eliminated, because glycerol and the borosilicate pipe have the same refractive indexes and so the light directly exposes to the fluid without any refraction.

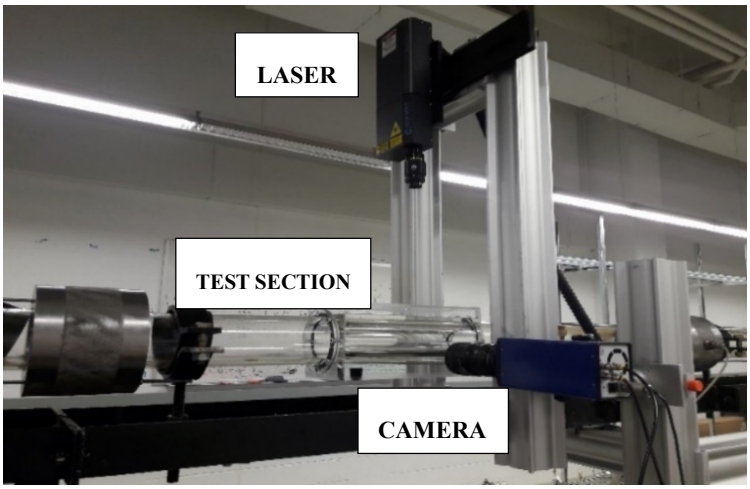

Figure 3. Image of the particle image velocimetry (PIV) setup and the test section.

PIV setup consisted of a New Wave Research Solo III Nd:YAG laser (New Wave Research 13900 NW Science Park Drive, Portland, OR USA 97229-5497), a Lavision Imager Intense CCD camera, and a Nikon 50 mm AF Nikkor lens (Nikon Inc. 1300 Walt Whitman Road Melville, NY 11747-3064, USA) of 1.4 mm aperture. The wavelength of the laser was 532 nm, and the Imager Intense was a double framed camera with a 12-bit CCD sensor of 1376 × 1040 pixels. All these components were monitored and synchronized by a commercial software, Davis 8.3. This software was also used to process and analyze the recorded data set. In addition, the status of the sand bed at critical flow rates or at some subcritical flow rates was recorded by a Samsung digital camera—8 MP, f/2.4, 31 mm, AF, 1080 p @ 30fps (105 Challenger Road Ridgefield Park, New Jersey 07660 USA).

2.4. Experimental Procedure

The experimental procedure consisted of three main stages: (i) the establishment of the sand bed; (ii) the polymer fluid circulation through the flow loop (over the sand bed), and the critical flow rate determination; (iii) the PIV measurements at a critical flow rate and at several subcritical flow rates. Prior to the bed erosion experiments, we conducted a calibration test to verify the accuracy of the pressure loss measurement. The method of verification of the frictional pressure loss measurement and the experimental procedure for the three main stages are briefly explained in Sections 2.4.1–2.4.3.

2.4.1. Verification of the Accuracy of the Frictional Pressure Loss Measurements

Frictional pressure drops for the water (no sand bed) flow in the horizontal flow loop were measured at various flow rates. Friction factors corresponding to these pressure loss measurements were determined by using the Fanning friction equation (Equation (3)). Calculated friction factors were then compared with theoretical values calculated from conventional pipe flow correlation [24] to confirm the accuracy of the pressure loss measurements. Figure 4 shows the results of the comparisons of the theoretical and experimental data:

$$\Delta P = f\frac{\rho u^2}{d}\Delta L \tag{3}$$

In Equation (3), ΔP is the frictional pressure drop, ΔL is the length of the pipe section over which the friction pressure loss was measured (3 m in this case), ρ is the fluid density, u is the bulk velocity, f is the friction factor and, d is the pipe inner diameter.

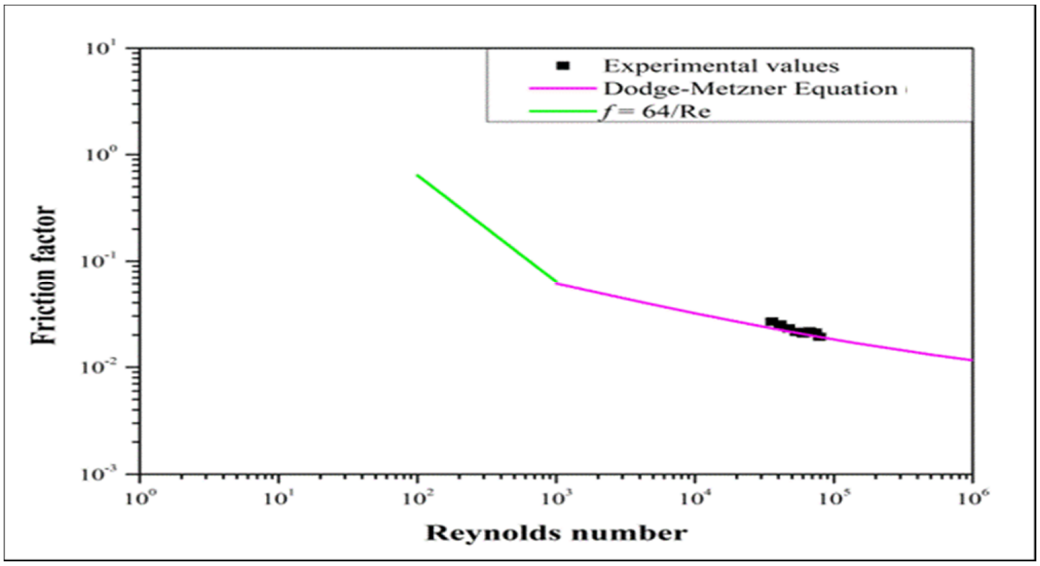

Figure 4. Comparison of the experimental friction factor values estimated from water-only flow tests against the ones calculated from the Dodge and Metzner equation [24].

2.4.2. Sand Bed Establishment

Initially, the suction tank was filled with water, which was circulated through the flow loop at the highest possible flowrate. Then, the sand particles were added to the tank, while the water was still in circulation. Effort was spent to get the initial bed height the same for all the experiments. The amount of sand needed to get the same bed height varied depending on the sand particle size. Depending on the particle mesh size range, the solid concentration used in the experiments changed from 5% to 8% wt/wt. When the sand bed was uniform, everywhere in the flow loop, the pump was stopped, and the valves at both ends of the pipe section were closed. The fluid was kept in the flow loop under

static condition overnight to make sure all the sand particles in suspension settled down and formed a continuous bed.

2.4.3. Polymer Fluid Circulation and Measurement of Critical Flowrate

After establishing a uniform bed, the suction tank was drained. In the mixing tank, the polymer fluid was prepared and circulated through the flow loop starting with the low (subcritical) flow rate and gradually increasing it to the level at which the first couple of particles start moving. When the movement of the first couple of sand particles were observed in rolling mode (i.e., the onset of the bed erosion), then the respective flow rate was recorded as the critical flow rate for bed erosion in that particular sand-size range. Frictional pressure losses were also recorded at the critical and the various subcritical flow rates. We did not consider any other mode (i.e., saltation, heterogeneous suspension, and homogeneous suspension) of solids transport in this study.

2.4.4. PIV Measurements

PIV is a non-intrusive laser-based optical measurement technique, commonly used to measure the instantaneous local (i.e., near-wall) fluid velocities and analyze the flow characteristics associated with the turbulent flow conditions [25]. In this technique, tracer particles sensitive to the light exposed to the laser beam and their movements (i.e., velocity and direction) are recorded by using a double frame high-speed CCD camera. The recorded images are converted into velocity field data via a computer analysis, which requires the use of a special software [26] allowing the data processing by fast Fourier transformation (FFT) technique [25].

The PIV setup consisted of a light source and a recording device. A double-pulse laser was used as the light source, and double-frame CCD camera was used as the recording device. The camera view plane must be orthogonal to the laser light as shown in Figure 3. The tracer particles were added to the suction tank while maintaining the polymer fluid circulation for a while to obtain a homogenous tracer distribution in the system. Hollow glass spheres with a mean diameter of 10 microns were used as the tracer particles in the current study. The density of the tracer particles were similar to the density of the fluid, so the tracers exactly followed the fluid flow. Since the flow was seeded with tracer particles, these tracer particles reflected the light when the laser light was impinged on them. The reflected light was then detected by the camera. Two successive images were captured by the camera in a very short time period.

Figure 5a shows typical PIV images acquired during the experiments. In this image, the cuttings bed is located at the bottom while the polymer fluid seeded with tracer particles (bright white dots) is flowing above the bed. These pictures were processed and converted into velocity field data by using a special software [26], which allows data processing by the Fast Fourier Transformation (FFT) technique [25]. The details of the PIV data processing procedure are provided in Section 2.5. PIV measurements at critical and subcritical flow rates were performed and recorded using the Davis 8.3 software. At least 1000 pairs of images were acquired for each flow experiment, and the velocity values were averaged out to ensure the higher accuracy of the measurements.

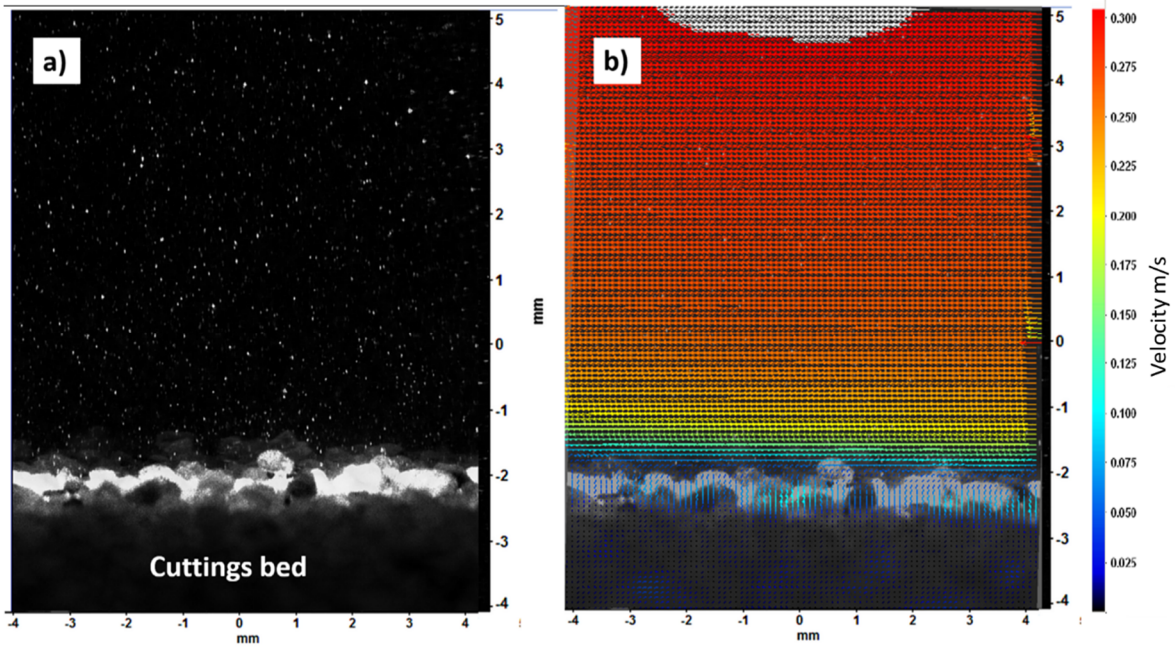

Figure 5. (**a**) Typical PIV image acquired during the tests, and (**b**) the resultant velocity field.

2.5. Data Processing and Analysis

The data processing and analysis consisted of two parts. In the first part, we determined the critical flow rate. The fluid flow over the stationary sand bed at various flow rates was recorded by the video camera. The fluid flow rate was gradually increased from very low subcritical flow rates to the critical flow rate where the first movement of the particles was observed. The critical flow rate was determined visually.

The second part was involved in the PIV data processing and analysis. The initially added light-sensitive tracer particles following the fluid flow were seen as the bright spots in each pair of captured PIV images (Figure 5a), and they were detected by the Davis 8.3 software. By cross-correlating this pair of images, the displacement (Δx and Δy) of the particles between the two images was determined [26]. Since the time interval between the two images was known, the instantaneous velocities ($\hat{\mathbf{u}}$: instantanous local velocity in the axial direction; $\hat{\mathbf{v}}$: instantanous local velocity in the radial direction) were calculated for all the detected points by using the particle displacement (Δx: displacement in the axial direction and Δy: displacement in the radial direction) and the time interval (Δt) as follows (Equation(4)):

$$\begin{cases} \hat{u} = \frac{\Delta x}{\Delta t} \\ \hat{v} = \frac{\Delta y}{\Delta t} \end{cases} \quad (4)$$

In order to determine the displacement of the detected bright spots in the x and y directions, Davis 8.3 software applied a FFT-based cross-correlation method [26]. First, both images were segmented into small interrogation windows and those windows in two images were compared to recognize the cross-correlation [26]. The exact displacement was determined by the identification of the highest peak of the correlation. A multi-pass approach starting from the window size of 64×64 down to 24×24 including the 32×32 size in between was used in the PIV image processing with an overlap of 50%. The recorded data with those settings were exported to excel files for further data analysis. Figure 5b shows the final velocity vector field for the flow over the cuttings bed.

Four main features of turbulent flow, Reynolds stresses, axial turbulence intensities, radial turbulence intensities and near-wall dimensionless velocities, were further analyzed and compared for all cases to detect the difference in the turbulent characteristics of the fluid flow over the sand bed. The Davis 8.3 software calculates all these features based on the governing equations using the velocities

and the velocity fluctuations measured in the x and y directions for each pair of images taken. The near-wall velocity profiles were presented in terms of dimensionless distance (y^+) and dimensionless velocity units (u^+) as defined by Equations (5) and (6), respectively.

$$y^+ = \frac{\rho y u_\tau}{\mu} \tag{5}$$

$$u^+ = \frac{u}{u_\tau} \tag{6}$$

$$u_\tau = \sqrt{\frac{\tau_b}{\rho}} \tag{7}$$

In Equations (5)–(7); y is the vertical distance from the pipe wall, u is the local flow velocity, μ is viscosity, u_τ is the friction (shear) velocity, τ_b is the interfacial bed shear stress (i.e., the shear stress at the fluid/sand bed interface), and ρ is the fluid density. The universal law of the wall states that the near-wall velocity profiles generally consist of three regions depending upon the dimensionless distance from the bed: the viscous sub-layer $y^+ < 5$, the buffer region $5 < y^+ < 30$ and the log-law region $y^+ > 30$. The universal plot of a velocity profile for a hydrodynamically smooth flow condition is given by Equation (8) [27].

$$u^+ = \left\{ \begin{array}{c} y^+ y^+ < 10 \\ 2.44 \ln(y^+) + 5.5 > 30 \end{array} \right\} \tag{8}$$

The Reynolds shear stress (or turbulent stress) arises due to velocity fluctuations (u′ and v′) in the flow and is defined according to Equation (9).

$$\tau_R = \rho \overline{u'v'} \tag{9}$$

The definition of the axial turbulence intensity is given by the Equation (10):

$$u_{rms} = \sqrt{\overline{u'u'}} \tag{10}$$

The axial turbulence intensity is critical in sand particle removal because it represents the level of velocity fluctuations. Recent studies have indicated the significance of turbulent velocity fluctuations in particle removal [19,20]. The radial component of turbulence intensity, v_{rms}, is of particular importance in solids transport and solids suspension. Kelessidis and Bandelis [28], based on the work of Davies [29], discussed the eddy fluctuation force, which is essential in keeping particles in suspension in turbulent flow. Davies [29] has shown that the eddy fluctuation force is proportional to radial velocity fluctuations. A higher level of radial velocity fluctuation results in a higher eddy fluctuation force. The definition of the radial turbulence intensity is given by the Equation (11):

$$v_{rms} = \sqrt{\overline{v'v'}} \tag{11}$$

3. Results

3.1. Frictional Pressure Drop Measured for the Polymer Fluid Flow over the Sand Bed

Table 2 summarizes the frictional pressure loss measurements for the flow of the polymer fluid over the sand beds of three different particle size ranges (20/40, 30/50, 40/70 mesh sizes) at the sub-critical velocity of 0.25 m/s. There are slight differences between the initial bed heights of each particle size range, which might affect the measured frictional pressure drops. To minimize the effect of the slight variation in the initial bed height, the flow rates were adjusted to have the same superficial velocity of 0.25 m/s for each test. The adjustment in the flow rates were made by considering the area open to the fluid flow above the sand bed. The equivalent diameter was calculated by assuming the area open for flow above the cuttings bed as a circle. At the subcritical fluid velocity of 0.25 m/s, the Reynolds

number was 4800. The critical Reynolds number in this case was 2113. Therefore, the flow regime was determined as turbulent.

Table 2. Frictional pressure drop measured at 0.25 m/s superficial velocity.

Sand Particle Mesh Size	Bed Height cm	Equivalent Diameter m	Flow Rate lpm	Frictional Pressure Loss Pa
20/40	3.65	0.0767	70.3	43
30/50	3.10	0.0802	76.0	35
40/70	3.31	0.0789	74.7	49

Figure 6 summarizes all the frictional pressure loss values measured over the stationary bed of sands using multiple flow rates. It is worth noting that the flow rates are converted into effective average (superficial) velocities by using the ratio of the flow rate to the area open for flow. The derivation of the equation used for the calculation of the area open for the flow above the sand bed is provided in Appendix A. The measured frictional pressure loss values for the flow over the 20/40 and 40/70 mesh size of sand particles were close to each other at all fluid velocities. The frictional pressure loss measurements over the bed of the 30/50 mesh size (intermediate size of the three tested sands) range particles, however, they were distinctly lower than that of the flow over the bed of 20/40 and 40/70 particle mesh size ranges. Clearly, the polymer fluid flow over the 30/50 mesh size sands presents a "drag reduction effect". We repeated this test several times and obtained the same result. We do not have any clear explanation of what causes the "drag reduction effect" in this case.

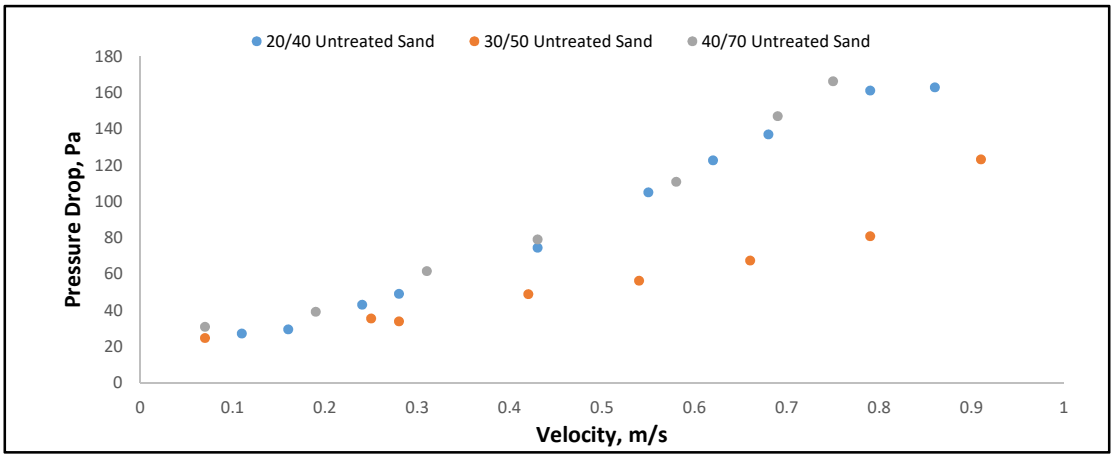

Figure 6. Frictional pressure drop measured for the flow of the polymer fluid over the sand bed of 3 different particle size ranges.

3.2. *Turbulent Flow Characteristics of Polymer Fluid Flow over the Sand Bed*

We compared the turbulent flow characteristics of polymer fluid flow over the sand bed of three different particle sizes using PIV measurements conducted at 0.25 m/s superficial fluid velocity.

In all the turbulent flow characteristics plots (Figures 7–10), the y coordinate represents the vertical distance from the bed (in the direction perpendicular to the flow) and y = 0 represents the sand bed–water interface.

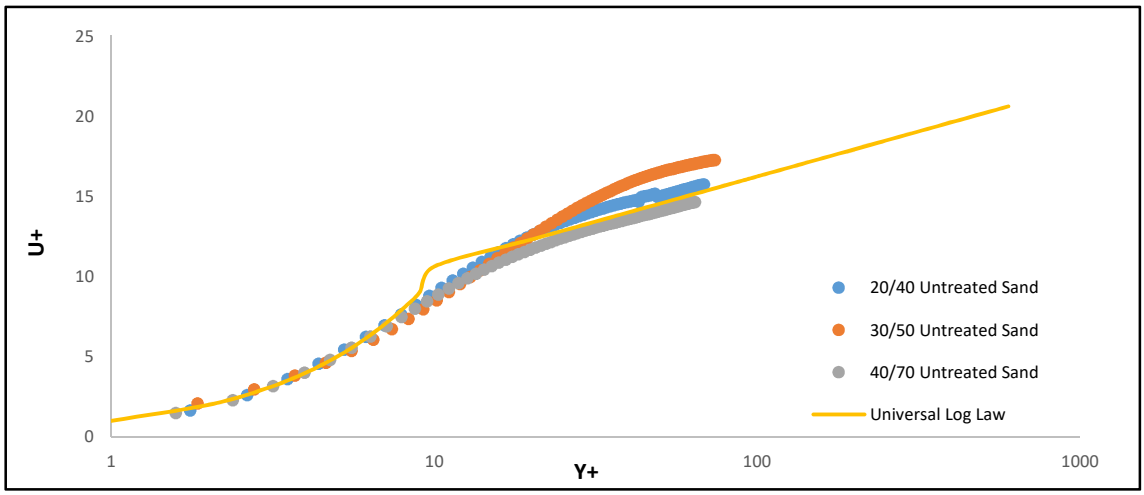

Figure 7. Near-wall (dimensionless) velocity profiles for the flow of the polymer fluid over the sand bed at a superficial velocity of 0.25 m/s.

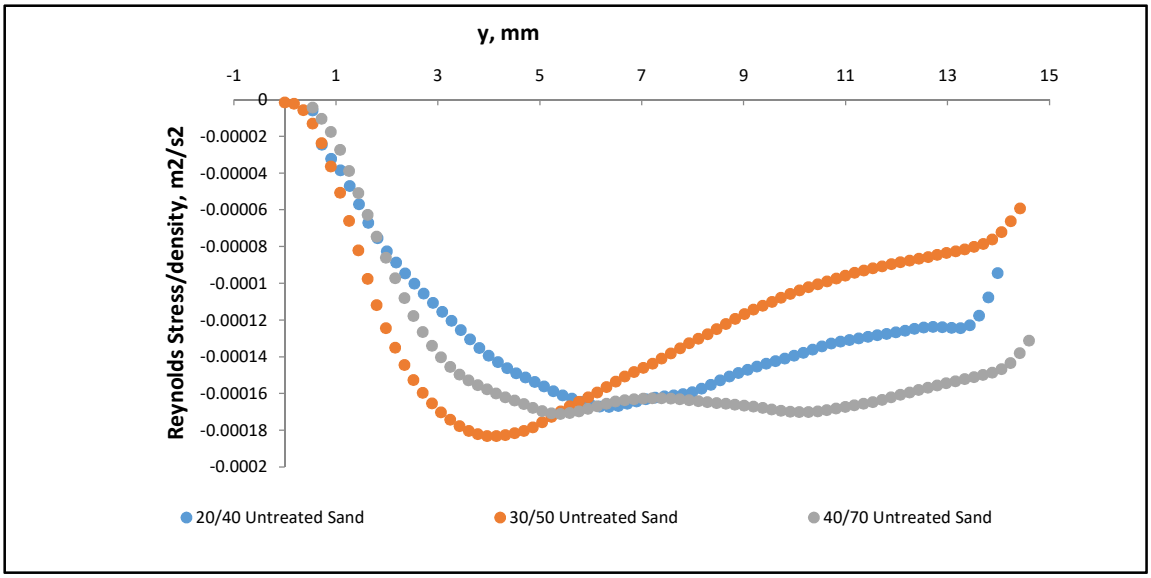

Figure 8. Reynolds stress profiles for the flow of polymer fluid over the sand bed at the superficial velocity of 0.25 m/s.

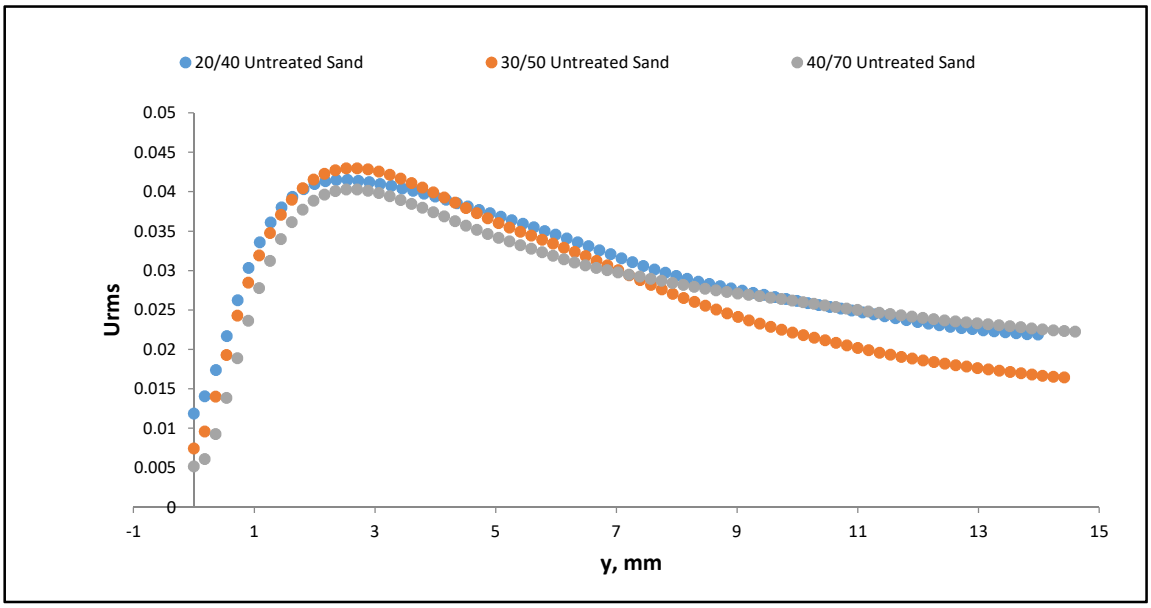

Figure 9. Axial turbulence intensity profiles for the flow of polymer fluid over the sand bed at the superficial velocity of 0.25 m/s.

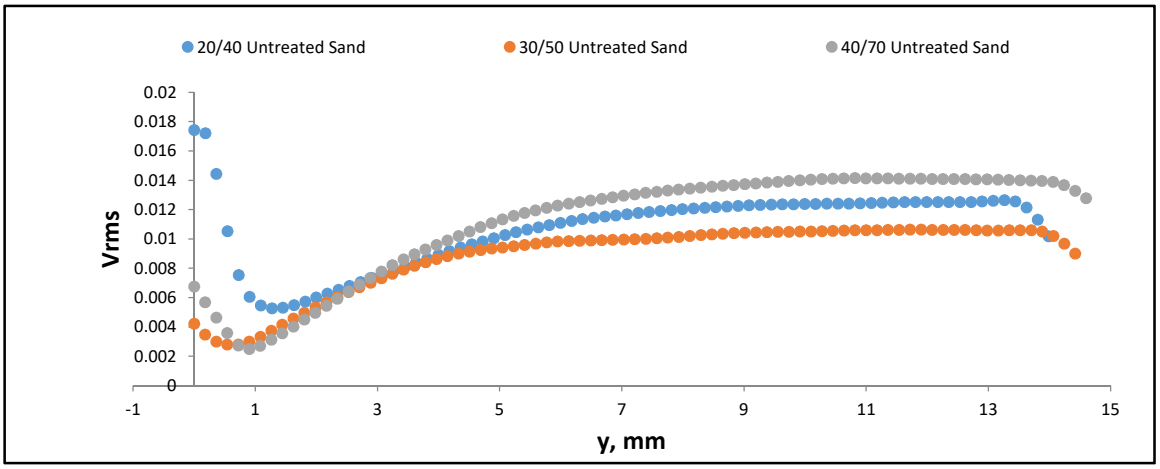

Figure 10. The radial turbulence intensity profile for the flow of polymer fluid over the untreated sand bed at the subcritical velocity of 0.25 m/s.

3.2.1. Near-Wall Velocity

Figure 7 summarizes the near-wall velocity profiles (presented in terms of dimensionless units). The near-wall velocity profile for the flow over the 40/70 mesh size for the untreated sand particles follows the universal law within the log-law region ($y^+ > 30$), indicating that the flow is hydrodynamically smooth in this case. The near-wall velocity profiles for the flow of the polymer fluid over the 20/40 and 30/50 mesh size sand bed were shifted up from the universal log-law trend line, indicating that the drag reduction effect prevails in these two cases. The drag reduction effect was more significant for the polymer fluid flow over the 30/50 mesh size sand bed. These results are in line with the direct measurement of frictional pressure losses presented earlier, where the lowest pressure drop was observed for the flow of the polymer fluid over the 30/50 mesh size sand bed.

3.2.2. Reynolds Shear Stress

Figure 8 presents the comparison of the normalized Reynolds shear stress profiles for the polymer fluid flow over the 20/40, 30/50 and 40/70 mesh size sand bed at the superficial velocity of 0.25 m/s. The near-wall Reynolds stress profiles for all three sands seemed to be very similar. However, if we take a closer look, we may say that the Reynolds stress registered at the bed ($y^+ = 0$) seems to be the lowest for the flow over the 30/50 mesh size sand beds, indicating a more effective momentum transfer from fluid to solids in this case. Again, this observation is in line with the lowest frictional pressure losses observed for the flow over the 30/50 sand size bed.

3.2.3. Axial Turbulence Intensity

Figure 9 shows the axial turbulence intensity profiles (also called the normal Reynolds stress) for the polymer fluid flow over the sand beds with three different mesh sizes of sands at the superficial velocity of 0.25 m/s. The axial turbulence intensity near the wall is slightly higher for a flow over the 20/40 mesh size bed than that of the cases with 30/50 and 40/70 mesh size sand beds, indicating a favorable flow condition for the removal of 20/40 mesh size particles.

3.2.4. Radial Turbulence Intensity

Figure 10 presents a comparison of the radial turbulent intensity profiles for the polymer fluid flow over the sand beds of three different particle size ranges at the superficial liquid velocity of 0.25 m/s. The lowest radial turbulent intensity was registered for the flow over the sand bed with particles in the 30/50 mesh size range, which indicates that for the flow over the 30/50 mesh size sands, turbulent eddies are in a more stable state (i.e., lower turbulence energy level). If the eddies are in a more stable state, this would reduce the frictional pressure losses due to the decreased turbulent energy and momentum transfer in the radial direction. These results are also in line with the observation of the lowest pressure drop registered for the flow over the 30/50 mesh size sand bed. The highest radial turbulent intensity value was obtained for the flow over the 20/40 particle size bed, indicating that more turbulent energy (higher eddy fluctuation forces) was available for particle removal in this case, which would be expected to improve the bed erosion performance.

3.2.5. Frictional Velocity

The frictional velocity is generally determined by analyzing the near-wall velocity data obtained from PIV measurements [30]. It is directly related to the interfacial bed shear stress (Equation (5)). The interfacial bed shear stress, τ_b, cannot be deduced accurately from frictional pressure loss data because more than one surface is involved in the flow (i.e., pipe wall and the bed surface). Therefore, the friction velocity, u_τ, cannot be directly estimated using the bed shear stress. In this study, we determined the friction velocity, u_τ, by using the plot of local instantaneous axial velocity (u) vs. the vertical distance (y) from the surface of the sand bed. These data were obtained directly from PIV measurements. The detailed procedure for determining the friction velocity from the PIV-measured velocity data is given elsewhere [30].

The interfacial bed shear stress is also an indirect measure of the total frictional pressure losses in the system. Therefore, the measured frictional pressure losses and the PIV-derived frictional velocities are expected to correlate well with each other. The variations of the frictional velocities with a sand particle size (as shown in Figure 11) are very much in line with that of the measured frictional pressure drop (shown in Table 2).

The lowest frictional pressure drop at the superficial velocity of 0.25 m/s was measured for the flow over the 30/50 mesh size sand bed. Similarly, the lowest frictional velocity value was derived from the analyses of the near-wall velocity data obtained from the PIV measurements during the polymer fluid flow over the 30/50 mesh size sand bed. The highest frictional pressure drop was measured for the flow over the 40/70 mesh size sand bed. Correspondingly, the highest frictional velocity value was

derived from the analyses of the near-wall velocity data obtained from the PIV measurements during the flow of the polymer fluid over the 40/70 mesh size sand bed.

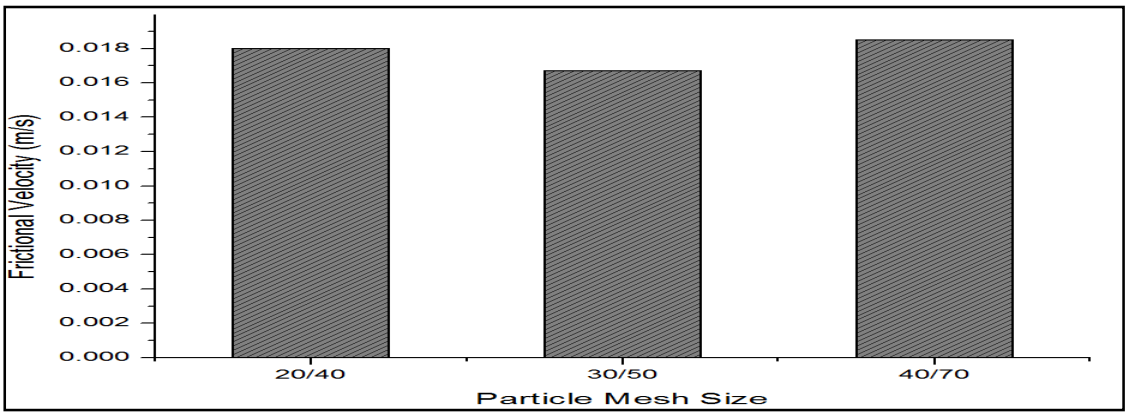

Figure 11. Friction velocity vs. the particle mesh size for the experiments conducted at the sub-critical velocity of 0.25 m/s.

3.3. Critical Velocity Required for the Particle Removal from the Sand Bed Size

Table 3 summarizes the critical velocities required for the onset of the particle removal from the sand bed using the polymer fluid. The lowest critical velocity was observed for the flow over the sand bed with the largest particle size (i.e., 20/40 mesh). For the flow over the sand bed with 30/50 and 40/70 mesh size particles, the critical velocity decreased with the decreasing sand size.

Table 3. Critical velocity required for the particle removal from the untreated sand bed.

Sand Mesh Size	Bed Height (cm)	Area Open for Flow (cm^2)	Critical Flow Rate (lpm)	Critical Velocity (m/s)	Critical Pressure Drop (Pa)
20/40	3.65	45.8	183.5	0.67	122.61
30/50	3.1	50.6	271.6	0.895	123.12
40/70	3.31	48.9	218.3	0.744	166.2

The fact that the lowest critical velocity was observed with the largest particle size within the group indicated that when a polymer-based drilling fluid was used for the solids transport, the critical velocity was not solely controlled by the absolute value of the particle size. To be able to explain this rather unexpected observation, we needed to conduct further analyses of the forces actually involved in this process.

3.3.1. Analyses of Forces Acting on the Particles during the Flow of Polymer Fluid over the Sand Bed

Rolling is the most common particle transport mechanism in highly inclined and horizontal wells [6]. In this study, we defined the critical velocity as the fluid velocity recorded at the onset of a particle removal from the bed deposits in rolling mode. Ramadan et al. [18] developed a mechanistic hole-cleaning model where they described the main driving forces behind the particle movement (in rolling mode) from a bed deposit in an inclined wellbore (Figure 12). Assuming a bed particle is at the threshold condition for rolling and neglecting the friction forces between the bed particles, Ramadan et al. [18] derived the rolling torque equation using the balance of the moments around the center of a spherical particle (Equation (12)). The rolling of particles along the bed occurs when the rolling torque becomes positive:

$$\Gamma_p = \frac{d_p}{2}\left(F_D \sin\phi + F_L \cos\phi - F_p \cos\phi - F_B \sin(\alpha + \phi)\right) \quad (12)$$

where:

Γ_p: rolling torque; d_p: particle diameter; F_D: drag force; F_L: lift force; F_p: plastic force
F_B: weight of particle in the fluid; α: hole inclination; ϕ: angle of repose

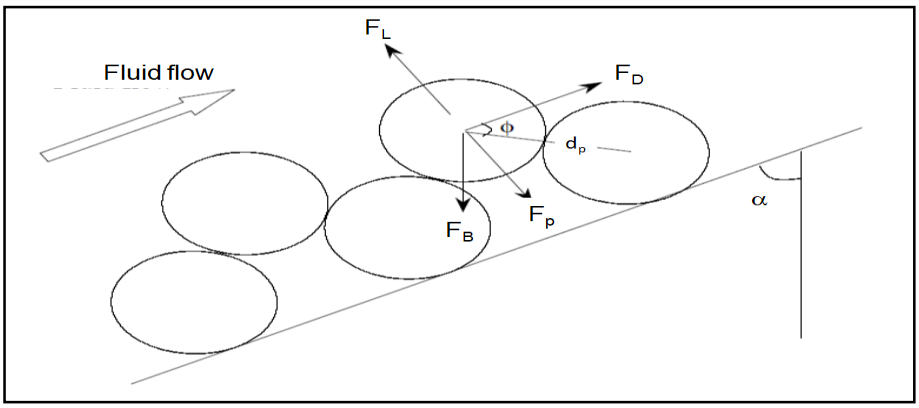

Figure 12. Forces acting on a single particle laying on a sand bed (Ramadan et al. [18]).

The fluid drag and lift forces are the major forces responsible for the particle movement. However, it was shown that the drag forces are generally in an order of magnitude higher than the lift forces [20]. Therefore, in our analyses of the particle movement, we neglected the effect of the lift forces. The drag force exerted by the flowing fluid on the sand particles was estimated by using the Equation (13) [20]:

$$F_D = \frac{1}{2}\rho A_p C_D u^2 \tag{13}$$

where F_D is the drag force, ρ is the fluid density, u is the local instantaneous axial fluid velocity, A_p is the projected area of the sand particle and C_D is the drag coefficient. The drag coefficient, C_D, is generally given as a function of the particle Reynolds number, Re_p. The particle Reynolds number for the pseudo plastic (power law) type fluids can be determined by using Equation (14).

$$Re_p = \frac{\rho u^{2-n} {d_p}^n}{K} \tag{14}$$

C_D values were determined by using the correlations (Equations (15)–(17)) suggested by Duan et al. [15]:

$$C_D = \frac{24}{Re_p}(2-n),\ Re_p < 0.2(2^n) \tag{15}$$

$$C_D = \frac{37}{\left(\frac{Re_p}{2^n}\right)^{1.03}} + n\left[1 - \frac{20.9}{\left(\frac{Re_p}{2^n}\right)^{1.11}}\right],\ 0.2(2^n) < Re_p < 24(2^n) \tag{16}$$

$$C_D = \frac{37}{\left(\frac{Re_p}{2^n}\right)^{1.03}} + 0.25 + 0.36n,\ 0.2(2^n) < Re_p < 100(2^n) \tag{17}$$

where Re_p is the particle Reynolds number, d_p is the particle diameter, K is the consistency index, n is the flow behavior index, u is the local instantaneous axial flow velocity, ρ the is fluid density and C_D is the drag coefficient.

The drag force (Equation (11)) is a direct function of the local instantaneous axial velocity, u. It was shown that the instantaneous local velocity (i.e., fluid velocity at the particle/fluid interface) could be significantly different than the average fluid velocity [20]. We used PIV measurements to determine

the instantaneous local (near-wall) axial velocity values. In order to calculate the drag force, we used the largest particle size within a given particle mesh size range.

In our analyses of particle movement, we considered the buoyed weight of the particle, F_B (i.e., the difference between the force of gravity, F_g, and the buoyancy force, F_b) as the main force resisting the particle movement (i.e., neglected the friction forces and the van der Vaals forces). The buoyed weight of the particle, F_B, can be estimated using the Equation (18):

$$F_B = F_g - F_b = 1/6\ \pi {d_p}^3 g\ (\rho_s - \rho_f) \quad (18)$$

where d_p is the particle size, g is the gravitational acceleration, ρ_s is the solid density, ρ_f is the fluid density.

F_p is the plastic force due to the yield stress of the fluid. The fluid used in our experiments was the power law type (showing very low or negligible yield stress), therefore, we did not consider the effect of the plastic forces. The inclination angle was 90 degrees (i.e., horizontal well). The bed was assumed to have a uniform deposition arrangement. The average angle of repose, ϕ, for uniformly deposited sand particles was measured as 30 degrees [18]. The particle movement can be initiated when the net-rolling torque becomes greater than zero. By introducing all the assumptions stated above into Equation (12), we could finally determine that the required condition for the initiation of the particles can be approximated as:

$$F_D > F_B \times \cos\Phi \quad (19)$$

The net force, F_N, acting on the particle, can be approximated by the difference between F_D and $F_B \times \cos\Phi$. A summary of the forces acting on a single sand particle at the critical velocity is provided in Table 4. For the 40/70 mesh size sand particles, the drag force could not be calculated due to a lack of PIV data for the critical velocity.

Table 4. Forces acting on a single sand particle at the critical velocity.

Particle Mesh Size	Particle Size Micron	Critical Velocity m/s	Near Bed Velocity m/s	C_D	F_D N	$F_B \times \cos\Phi$ N	Net Force N
20/40	840	0.670	0.038	5.331	4.10×10^{-6}	3.51×10^{-6}	5.93×10^{-7}
30/50	590	0.895	0.036	7.065	2.57×10^{-6}	1.21×10^{-6}	1.36×10^{-6}
40/70	420	0.744	-	-	-	5.07×10^{-7}	-

Results shown in Table 4 indicate that although the critical velocity (calculated using the average flow rate measured at the onset of the particle removal from the bed and the area open for flow above the sand bed) for the 20/40 mesh size sand is lower than that of the 30/50 mesh size sand; the near-wall velocity (measured by PIV) for the 20/40 mesh size sand was actually higher than that of the case with the 30/50 mesh size. The drag force (Equation (10)) acting on the particle was controlled by the near-wall velocity, not by the average velocity. Although the critical velocity was the lowest for the onset of the 20/40 mesh size particle movement, the corresponding drag force was the highest in this case. The non-zero net force ($=F_D - F_B \times \cos\Phi$) also confirms that the drag force was sufficiently high to mobilize the 20/40 particles at this lower critical velocity (0.67 m/s).

We also calculated the forces acting on a single sand particle at sub-critical velocities and the results were summarized in Table 5. The net forces were negative in all cases, confirming that the sand particles could not be mobilized at these sub-critical velocities.

As shown by the results presented in Table 5, the 30/50 mesh size sands were not mobilized at the superficial velocity of 0.778 m/s, which was actually higher than the critical velocity observed for the 20/40 mesh size sands (0.67 m/s). When we compared the near-bed velocities for these two cases, we saw that although the critical velocity for the 20/40 mesh size sand (0.67 m/s) was lower than the sub-critical velocity (0.778 m/s) for the 30/50 mesh size sand, the near-bed velocity measured in the former case (0.03824 m/s) was higher than that of the latter (0.01358 m/s).

Table 5. Forces acting on a single untreated sand particle at sub-critical velocity.

Particle Mesh Size	Particle Size Micron	Superficial Velocity m/s	Near Bed Velocity m/s	C_D	F_D N	$F_B \times \cos\Phi$ N	Net Force N
20/40	840	0.6	0.02387	7.955	2.51×10^{-6}	3.51×10^{-6}	-1.00×10^{-6}
30/50	590	0.778	0.01358	18.094	9.12×10^{-7}	1.21×10^{-6}	-3.00×10^{-7}
40/70	420	0.436	0.01026	31.578	4.60×10^{-7}	4.80×10^{-7}	-2.00×10^{-8}

These results also confirm that near-bed velocities (controlling the drag forces) vary depending on the relative size and position of the sand particle with respect to the viscous boundary layer thickness. In the following section, we will try to quantify the boundary layer thickness and compare it to the particle size so that we can determine the relative position of the sand particles in each case with respect to boundary layer thickness.

3.3.2. Boundary Layer Thickness

The lowest critical velocity observed for the 20/40 mesh size particles can be explained by the effective drag forces acting on the particles, which may vary significantly depending on the relative positions of the particles within this size range (420–840 micron) with respect to the viscous boundary layer thickness, δ_v (Equation (20)) [27].

$$\delta_v = \frac{5\mu_w}{\rho u_\tau} \tag{20}$$

where δ_v is the boundary layer thickness, μ_w is the fluid viscosity at the wall, ρ is the fluid density, and u_τ is the friction velocity. Viscous sublayer thickness estimated for the polymer fluid flow over the three different mesh size sand beds at the corresponding critical flow rates are presented in Table 6.

Table 6. Viscous sublayer thickness for the polymer fluid flow over the sand bed at their corresponding critical flow rates.

	20/40 Sand	30/50 Sand	40/70 Sand
Particle Mesh Size (micron)	840–420	590–297	420–210
Viscous Sublayer Thickness (micron)	765	811	797

The estimated boundary layer thickness at the critical velocity of 20/40 mesh size particles (0.67 m/s) was 765 microns. It was smaller than the largest particle size in the group (i.e., 840 microns), therefore, we could expect that some of the particles within the 20/40 mesh size range would stick out of the boundary layer and hence, could be exposed to higher local velocities (as opposed the ones positioned completely within the boundary layer). This was exactly what we observed as shown by the PIV data measured near the wall (Table 4). As a result, higher effective drag forces were active on the 20/40 mesh size particles, which mobilized the particles at lower average superficial velocities (Table 4).

It is worth noting that the estimated viscous boundary layer thickness (i.e., 765 microns) at the critical velocity of the 20/40 mesh size particles (i.e., 0.67 m/s), was higher than the largest size particles within the group of the 30/50 mesh size (i.e., 590 microns) and the 40/70 mesh size (i.e., 420 microns) particles. That means that the 30/50 and 40/70 mesh size particles were all located within the viscous boundary layer at this critical velocity, which was able to erode the 20/40 mesh size sand bed. Therefore, the effective velocity (and the drag force) acting on the 30/50 and 40/70 mesh size particles might have not been high enough to mobilize these particles at this velocity.

As indicated by the data shown in Table 6, boundary layer thicknesses corresponding to the critical velocities of the 30/50 (811 microns) and 40/70 (797 microns) mesh size particles were all greater than the largest particle size in each group (590 microns and 420 microns, respectively), which means that both the 30/50 and 40/70 mesh size particles were located within the viscous boundary layer when the particles started to move. Since both the 30/50 and 40/70 mesh size particles were sitting in the

viscous sublayer, they would be exposed to relatively lower instantaneous local velocities at the onset of the particle movement. However, the 30/50 size particles have a relatively larger size, and therefore, holding forces (mainly gravity and friction forces) would be higher in this case and they would need higher drag forces (and hence higher local velocities within the boundary layer) to be mobilized as compared to the 40/70 size particles (smaller size particles mean that the holding forces are smaller and that they require a smaller drag force and lower local velocities to be mobilized). That would be the reason why the critical velocity of the 30/50 mesh size particles was higher than that of the 40/70 mesh size sand particles.

4. Conclusions

An experimental study was conducted to investigate the possible effects of sand particle size on the critical velocity, the frictional pressure drop and the turbulent characteristics of the polymer fluid flow over a sand bed deposit in a horizontal pipe.

Frictional pressure drop (measured at the same average fluid velocity of 0.25 m/s) for the flow of polymer fluid over the 30/50 mesh size sand was significantly lower than that of the ones with the 20/40 and 40/70 mesh size of sand beds. The near-wall velocity profile for the flow of the polymer fluid over the 30/50 mesh size sand bed also confirmed that the drag reduction effect prevails in this case. However, the critical velocity for the 30/50 mesh size particle removal was higher than that that of the case with the 20/40 and 40/70 mesh size sand bed.

The lowest critical velocity was observed for the polymer fluid flow over the bed with the largest particle size range (i.e., 20/40 mesh size of sand). The highest Reynolds stress, axial and radial turbulent intensities recorded in this case all created favorable conditions for the effective removal of the 20/40 mesh size particles. These results also confirm the well known positive impact of the turbulent flow on the hole-cleaning efficiency.

When a polymer-based drilling fluid is used for solids transport, the critical velocity not only depends on the absolute value of the particle size but also on the relative position of the sand particle with respect to the viscous sublayer thickness (i.e., how the particle size compares with the viscous sublayer thickness).

From the practical field application point of view, these results suggest that although the use of dilute polymer fluids for hole cleaning in horizontal wells may cause drag reduction, it may impede the hole-cleaning performance, especially when the drill cuttings size are relatively small (e.g., fine sand particles).

Author Contributions: M.M.H.: carried out most of the research (conducted experiments, analyses of the data, wrote original draft of the paper) as part of his MSc research study. S.K.A.: provided help with designing and conducting the experiments and the design of the fluids. E.K.: provided the supervision of the MSc study, funding acquisition, analyzed the data, read and revised the manuscript. All authors have read and agreed to the published version of the manuscript.

Funding: This research is financially supported by the funds available from the Natural Sciences and Engineering Research Council of Canada (NSERC EGP 515333-17 Kuru).

Acknowledgments: Authors would like to thank 3M Canada Company for providing us the sand samples used in this research. We also would like to thank Genaro Gelves and Ibrahim Al-Rafia of 3M Canada Company for their support and valuable discussions they provided throughout this project.

Conflicts of Interest: The authors declare no conflict of interest. The funders had no role in the design of the study; in the collection, analyses, or interpretation of data; in the writing of the manuscript, or in the decision to publish the results.

Appendix A. Model for Calculations of Hydraulic Diameter and Annular Area Open for Flow with the Presence of the Cuttings Bed Deposit

The hydraulic diameter and annular cross-sectional area available for fluid flow in the presence of sand bed are defined in the following section.

Because variation in the bed height might affect flow velocities and the measured frictional pressure drops over the sand bed, special attention was given to keep the bed height constant during the sand bed establishment in all the experiments. However, this was not a trivial task, but we managed to keep the bed height variation within the 3–10% range. Figure A1 shows the longitudinal and the cross-sectional views of the horizontal pipe with the presence of stationary sand deposits.

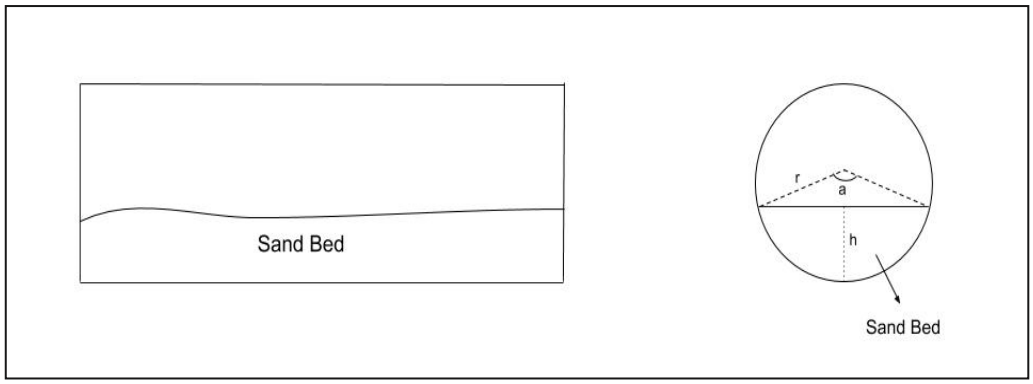

(**a**) (**b**)

Figure A1. (**a**) Sand bed profile along the horizontal pipe and (**b**) the cross-sectional view of the pipe with the sand bed [31].

In order to calculate the flow velocities in the pipe with the presence of sand bed, only the area above the sand bed open for water flow was considered. The open area (OA) available for the water flow above the bed was calculated by using Equation (A1):

$$OA = \frac{(360 - a)\Pi r^2}{360} + \frac{1}{2}\sin(a)r^2 \quad \text{(A1)}$$

The parameter a is defined by the Equation (A2):

$$a = 360 \times \frac{\text{Perimeter covered by the sand bed}}{\text{Perimeter of the pipe}} \quad \text{(A2)}$$

For the calculation of parameter a; the perimeter covered by the sand bed was physically measured. The perimeter of the pipe was simply 2ΠIr.

The hydraulic diameter was then calculated by assuming that area open for flow as a circle (Equation (A3)):

$$d_h = \frac{\text{Open Area (OA)}}{\text{Wetted Perimeter}} \quad \text{(A3)}$$

References

1. Nazari, T.; Hareland, G.; Azar, J.J. Review of Cuttings Transport in Directional Well Drilling: Systematic Approach. In Proceedings of the SPE Western Regional Meeting, Anaheim, CA, USA, 27–29 May 2010. [CrossRef]
2. Li, J.; Luft, B. Overview of Solids Transport Studies and Applications in Oil and Gas Industry—Experimental Work. In Proceedings of the SPE Russian Oil and Gas Exploration & Production Technical Conference and Exhibition, Moscow, Russia, 14–16 October 2014. [CrossRef]
3. Li, J.; Luft, B. Overview Solids Transport Study and Application in Oil-Gas Industry-Theoretical Work. In Proceedings of the International Petroleum Technology Conference, Kuala Lumpur, Malaysia, 10–12 December 2014. [CrossRef]

4. Brown, N.; Bern, P.; Weaver, A. Cleaning Deviated Holes: New Experimental and Theoretical Studies. In Proceedings of the SPE/IADC Drilling Conference, New Orleans, LA, USA, 28 February–3 March 1989. [CrossRef]
5. Martins, A.; Sa, C.; Lourenço, A.; Freire, L.; Campos, W. Experimental Determination of Interfacial Friction Factor in Horizontal Drilling with a Bed of Cuttings. In Proceedings of the SPE Latin America/Caribbean Petroleum Engineering Conference, Port-of-Spain, Trinidad, 23–26 April 1996. [CrossRef]
6. Martins, A.; Campos, W.; Liporace, F.; Wei, X.; Van Riet, E. On the Erosion Velocity of a Cuttings Bed During the Circulation of Horizontal and Highly Inclined Wells. In Proceedings of the SPE LACPEC, Rio de Janeiro, Brazil, 30 August–3 September 1997.
7. Adari, R.; Miska, S.; Kuru, E.; Bern, P.; Saasen, A. Cuttings Bed Erosion Curves Help Predict Optimum Circulation Time for Hole Cleaning. In Proceedings of the ETCE/ OMAE Joint Conference of ASME, New Orleans, LA, USA, 14–17 February 2000.
8. Cho, H.; Shah, S.N.; Osisanya, S.O. Selection of Optimum Coiled-Tubing Drilling Parameters Through the Cuttings-Bed Characterization. In Proceedings of the SPE/ICoTA Coiled Tubing Roundtable, Houston, TX, USA, 7–8 March 2001. [CrossRef]
9. Ozbayoglu, M.E.; Ettehadi Osgouei, R.; Ozbayoglu, A.; Yuksel, E. Estimation of Very-Difficult-to-Identify Data for Hole Cleaning, Cuttings Transport and Pressure Drop Estimation in Directional and Horizontal Drilling. In Proceedings of the IADC/SPE Asia Pacific Drilling Technology Conference and Exhibition, Ho Chi Minh City, Vietnam, 1–3 November 2010. [CrossRef]
10. Petersen, J. Determining the Cuttings Critical Transport Fluid Velocity using Simple Geometrical Approximations. In Proceedings of the SPE Bergen One Day Seminar, Bergen, Norway, 22 April 2015. [CrossRef]
11. McClure, M. Bed load proppant transport during slick water hydraulic fracturing: Insights from comparisons between published laboratory data and correlations for sediment and pipeline slurry transport. *J. Pet. Sci. Eng.* **2020**, *161*, 599–610. [CrossRef]
12. Brannon, H.D.; Wood, W.D.; Wheeler, R.S. The Quest for Improved Proppant Placement: Investigation of the Effects of Proppant Slurry Component Properties on Transport. In Proceedings of the SPE Annual Technical Conference and Exhibition, Dallas, TX, USA, 9–12 October 2005. [CrossRef]
13. Patankar, N.A.; Joseph, D.; Wang, J.; Barree, R.; Conway, M.; Asadi, M. Power law correlations for sediment transport in pressure driven channel flows. *Int. J. Multiph. Flow* **2002**, *28*, 1269–1292. [CrossRef]
14. Wang, J.; Joseph, D.; Patankar, N.; Conway, M.; Barree, R. Bi-power law correlations for sediment transport in pressure driven channel flows. *Int. J. Multiph. Flow* **2003**, *29*, 475–494. [CrossRef]
15. Duan, M.; Miska, S.; Yu, M.; Takach, N.; Ahmed, R.; Zettner, C.M. Critical Conditions for Effective Sand-Sized Solids Transport in Horizontal and High-Angle Wells. *SPE Drill. Complet.* **2009**, *24*, 229–238. [CrossRef]
16. Thomas, R.; Azar, J.; Becker, T. Drillpipe Eccentricity Effect on Drilled Cuttings Behavior in Vertical Wellbores. *J. Pet. Technol.* **1982**, *34*, 1929–1937. [CrossRef]
17. Bizhani, M.; Kuru, E. Particle Removal From Sandbed Deposits in Horizontal Annuli Using Viscoelastic Fluids. *SPE J.* **2018**, *23*, 256–273. [CrossRef]
18. Ramadan, A.; Skalle, P.; Johansen, S. A mechanistic model to determine the critical flow velocity required to initiate the movement of spherical bed particles in inclined channels. *Chem. Eng. Sci.* **2003**, *58*, 2153–2163. [CrossRef]
19. Diplas, P.; Dancey, C.L.; Celik, A.O.; Valyrakis, M.; Greer, K.; Akar, T. The Role of Impulse on the Initiation of Particle Movement Under Turbulent Flow Conditions. *Science* **2008**, *322*, 717–720. [CrossRef] [PubMed]
20. Bizhani, M.; Kuru, E. Critical Review of Mechanistic and Empirical (Semimechanistic) Models for Particle Removal From Sandbed Deposits in Horizontal Annuli With Water. *SPE J.* **2018**, *23*, 237–255. [CrossRef]
21. Rabenjafimanantsoa, A.; Time, R.W.; Saasen, A. Simultaneous UVP and PIV Measurements Related to Bed Dunes Dynamics and Turbulence Structures in Circular Pipes. In Proceedings of the 5th International Symposium on Ultrasonic Doppler Methods for Fluid Mechanics and Fluid Engineering, Zurich, Switzerland, 12–14 September 2006.
22. Hirpa, M.M.; Arnipally, S.K.; Bizhani, M.; Kuru, E.; Gelves, G.; Al-Rafia, I. Effect of Particle Size and Surface Properties on the Sandbed Erosion with Water Flow in a Horizontal Pipe. *SPE J.* **2020**, *25*, 1096–1112. [CrossRef]

23. Cengel, Y.A.; Cimbala, J.M. *Fluid Mechanics: Fundamentals and Applications*, 1st ed.; McGraw-Hill Higher Education: Boston, MA, USA, 2006; pp. 321–329, ISBN 978-0072472363.
24. Dodge, D.W.; Metzner, A.B. Turbulent flow of non-newtonian systems. *AIChE J.* **1959**, *5*, 189–204. [CrossRef]
25. Raffel, M.; Willert, C.E.; Kompenhans, J. *Particle Image Velocimetry: A Practical Guide*, 3rd ed.; Springer: Berlin/Heidelberg, Germany, 2018.
26. LaVision, Davis 8.3 Product Manual. 2015 Edition. Available online: https://www.lavision.de/en/products/davis-software/ (accessed on 1 April 2020).
27. Kundu, P.K.; Cohen, I.M.; Dowling, D.R. *Fluid Mechanics*, 5th ed.; Elsevier: Amsterdam, The Netherland, 2012.
28. Kelessidis, V.; Bandelis, G. Flow Patterns and Minimum Suspension Velocity for Efficient Cuttings Transport in Horizontal and Deviated Wells in Coiled-Tubing Drilling. *SPE Drill. Complet.* **2004**, *19*, 213–227. [CrossRef]
29. Davies, J. Calculation of critical velocities to maintain solids in suspension in horizontal pipes. *Chem. Eng. Sci.* **1987**, *42*, 1667–1670. [CrossRef]
30. Bizhani, M. Experimental and Theoretical Investigations of Particle Removal from Sand Bed Deposits in Horizontal Wells Using Turbulent Flow of Water and Polymer Fluids. Ph.D. Thesis, University of Alberta, Edmonton, AB, Canada, 2017.
31. Hirpa, M.M. Experimental Investigation of the Effects of Fluid Elastic Properties, Sand Particle Size and Surface Properties on the Bed Erosion Dynamics of the Sand Bed Deposited in Horizontal Pipeline. Master's Thesis, University of Alberta, Edmonton, AB, Canada, 2019.